

Strong multipolar transition enhancement with graphene nanoislands F

Cite as: APL Photonics 6, 086103 (2021); <https://doi.org/10.1063/5.0053234>

Submitted: 06 April 2021 . Accepted: 19 July 2021 . Published Online: 02 August 2021

 Gilles Rosolen, and  Bjorn Maes

COLLECTIONS

F This paper was selected as Featured



View Online



Export Citation

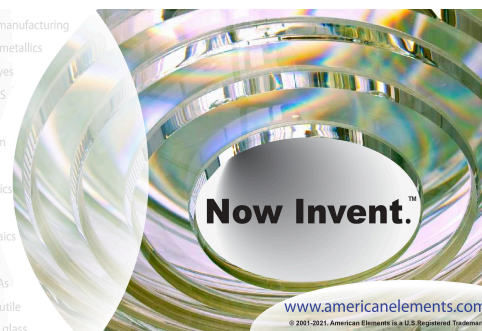


CrossMark



yttrium iron garnet glassy carbon beamsplitters fused quartz additive manufacturing
 zeolites III-IV semiconductors gallium lump copper nanoparticles organometallics
 nano ribbons barium fluoride europium phosphors photonics infrared dyes
 epitaxial crystal growth ultra high purity materials transparent ceramics CIGS
 cerium oxide polishing powder surface functionalized nanoparticles MRE grade materials thin film
 beta-barium borate rare earth metals quantum dots OLED lighting solar energy
 sputtering targets fiber optics
 scintillation Ce:YAG h-BN deposition slugs
 laser crystals CVD precursors photovoltaics
 lithium niobate InAs wafers
 dysprosium pellets MOFs AuNPs
 chalogenides ZnS CdTe
 perovskite crystals transparent ceramics

The Next Generation of Material Science Catalogs



www.americanelements.com
 © 2001-2021, American Elements Inc. a U.S. Registered Trademark



Strong multipolar transition enhancement with graphene nanoislands

Cite as: APL Photon. 6, 086103 (2021); doi: 10.1063/5.0053234

Submitted: 6 April 2021 • Accepted: 19 July 2021 •

Published Online: 2 August 2021



View Online



Export Citation



CrossMark

Gilles Rosolen^{a)}  and Bjorn Maes 

AFFILIATIONS

Micro and Nanophotonic Materials Group, Research Institute for Materials Science and Engineering, University of Mons, Place du Parc 20, 7000 Mons, Belgium

^{a)} Author to whom correspondence should be addressed: gilles.rosolen@umons.ac.be

ABSTRACT

For a long time, the point-dipole model was a central and natural approximation in the field of photonics. This approach assumes that the wavelength is much larger than the size of the emitting atom or molecule so that the emitter can be described as a single or a collection of elementary dipoles. This approximation no longer holds near plasmonic nanostructures, where the effective wavelength can reach the nanometer-scale. In that case, deviations arise and high-order transitions, beyond the dipolar ones, are not forbidden anymore. Typically, this situation requires intensive numerical efforts to compute the photonic response over the spatial extent of the emitter wavefunctions. Here, we develop an efficient and general model for the multipolar transition rates of a quantum emitter in a photonic environment by computing Green's function through an eigen permittivity modal expansion. A major benefit of this approach is that the position of the emitter and the permittivity of the material can be swept in a rapid way. To illustrate, we apply the method on various forms of graphene nanoislands, and we demonstrate a local breakdown of the selection rules, with quadrupolar transition rates becoming 100 times larger than dipolar ones.

© 2021 Author(s). All article content, except where otherwise noted, is licensed under a Creative Commons Attribution (CC BY) license (<http://creativecommons.org/licenses/by/4.0/>). <https://doi.org/10.1063/5.0053234>

I. INTRODUCTION

Usually the quantum emitter is approximated as a point emitting a dipolar electric field. This is a legitimate approximation when the wavelength of the emitted light is much larger than the size of the atom or molecule. In that case, high-order transitions (transitions beyond the dipolar one, such as two-photon processes and electric and magnetic multipolar transitions) are negligible and termed forbidden. However, these transitions are of particular importance in spectroscopy, photochemistry, quantum information, and many other fields. Here, we develop a numerical method that computes the multipolar transition rates of a quantum emitter in a general photonic environment, and we show that graphene nanoislands can locally break the conventional selection rules of a hydrogen-like emitter.

The transitions are governed by the coupling between the charged constituents of the emitter and the electromagnetic field. In free space, the latter is a plane wave, with expansion $\exp(i\mathbf{k} \cdot \mathbf{x}) \approx 1 + i(\mathbf{k} \cdot \mathbf{x}) - 0.5(\mathbf{k} \cdot \mathbf{x})^2 + \dots$ in the limit of $\mathbf{k} \cdot \mathbf{x} \rightarrow 0$. Through Fermi's golden rule, each term, which corresponds to a number of gradients of the electromagnetic field (0, 1, 2, ...), can be

traced back to a particular multipolar transition.¹ For visible light, the wave vector is $|\mathbf{k}| = 10^7 \text{ m}^{-1}$, and for hydrogen-like atoms, $\langle |\mathbf{x}| \rangle \approx 10^{-10} \text{ m}$. It directly shows that the first term in the Taylor expansion, attributed to the dipolar transition, dominates by 3 orders of magnitude compared to the linear order, attributed to the quadrupolar transition, and by 6 orders of magnitude compared to the quadratic term, attributed to the octupolar transition.² Therefore, stronger field gradients over the spatial extent of the wave function of the emitter are necessary to enhance higher-order transitions.¹

One route toward non-negligible higher-order terms is, therefore, to consider larger emitters, as shown for quantum dots³ and Rydberg excitons.⁴ Another route consists of enhancing the wave vector magnitude $|\mathbf{k}|$ by confining light in a nanophotonic structure. The wave vector can be written as $\mathbf{k} = \eta_0 \omega / c$, with the confinement factor η_0 being the ratio between the vacuum and the effective wavelength. In this case, higher-order transitions are enhanced by a factor η_0 to the power of the considered order (for example, the octupolar transition is enhanced by a factor η_0^2).⁵

Under these conditions, plasmonic nanoantennas are ideal candidates to enhance higher order transitions. For instance, in noble

metals, forbidden quadrupolar transitions are enhanced for emitters close to tips,⁶ interfaces,⁷ nanowires,⁸ nanogaps,⁹ arrays,¹⁰ and gold dimers.^{2,11,12} The strongly confined graphene plasmons ($\eta_0 = 150\text{--}300$, depending on the absorption losses^{13,14}) form an excellent platform for high-order transitions, which can occur efficiently, even similar to dipolar transitions.⁵ In the case of extremely high confinement ($\eta_0 > 500$) of plasmons in a two-dimensional material sheet, higher-order transition rates can surpass lower order transitions, hence breaking the conventional selection rules.^{5,15}

Generally, accessing high-orders allows us to probe a much larger range of the electronic energy level structure of an emitter, finding a way to a multiplex and broadband spectroscopy platform.^{5,11} These higher-order transitions already play an important role in spectroscopy of many relevant chemical species, from individual atoms^{16,17} to larger molecules with high symmetry, such as dihydrogen, carbon dioxide, methane, and benzene.^{18,19} In photochemistry, enhancing the magnetic dipole transition in oxygen is interesting for photochemical reactions.²⁰ Finally, interference effects between multipolar orders can occur: the possibility of complete suppression of a certain transition through interference is required for many applications in the context of quantum computing, quantum storage, and quantum communication.^{3,21}

Despite its high potential and these developments, the field is currently limited by the difficulty in computing the electromagnetic environment of the emitter. Indeed, computing the spontaneous emission rates of a quantum emitter requires the knowledge of the electromagnetic field profile over the spatial extent of the wavefunctions of the emitter.²² Usually, the problem is solved for absorption rates: in that case, a plane wave excites a nanophotonic structure and the near-field is extracted.^{1,6,9,10} This is a straightforward routine for conventional numerical methods, such as the finite-element method^{23,24} or the finite-difference time-domain method.²⁵ For spontaneous emission, however, the knowledge of the vacuum field is essential. As a first approximation, one can resort to symmetric problems²⁶ or consider only the relevant (properly quantized) modes of the structure for the process.^{2,8,11} The complete resolution, however, requires knowledge of Green's function, which is analytical only for uniform media and for simple geometries.^{5,15} Numerical evaluation is very demanding with conventional numerical methods, as repeated simulations for different positions and orientations of a point dipole source are necessary.¹²

In order to compute advanced photonic structures, a modal-based approach is very useful: a single simulation that determines the modes (e.g., of a cavity) is required to know the full spatial variation of Green's function.²⁷ The eigen permittivity modal expansion is particularly suited for the spontaneous emission of an emitter for which the emission frequency is fixed. Eigen permittivity modes have a permittivity eigenvalue that pertains only to a scattering element, which spans a finite portion of space. As a result, the normalization is trivial. Furthermore, they are orthogonal and appear to form a complete set.^{28,29} Once computed for a scatterer at a fixed wavelength, they straightforwardly give the optical response for any material constituting this scatterer. These modes have been derived during the 1970s in the quasi-static approximation, and were used to derive bounds for scattering problems,³⁰ to study spasers,³¹ disordered media,³² and second harmonic generation.³³ The formalism (called GENOME for GEneralized NOrmal Mode Expansion) was

recently extended beyond the quasistatic approximation by computing the electromagnetic fields and the associated Green's function of open and lossy electromagnetic systems, in particular for general nanoparticle configurations using commercial software (COMSOL Multiphysics).²⁹

In this paper, we derive a general method to compute the transition rate of a quantum emitter influenced by its electromagnetic environment in the weak coupling regime (Sec. II). We apply the macroscopic QED formalism, which separates the electromagnetic environment obtained from the classical Maxwell equations (we use GENOME to determine Green's function) from the quantum description of the emitter embodied by its wavefunction, which in this case is a hydrogen-like emitter. Then, we apply this method to compute the electric dipolar, quadrupolar, and octupolar transition rates of the emitter in the vicinity of graphene nanoislands with different geometries (triangle, square, and crescent), showing strong enhancement of the transition rates (Sec. III A). Afterward, we show that the graphene doping can be tuned to select particular transitions in Sec. III B, before demonstrating a local breakdown of the selection rules in Sec. III C.

II. METHOD

We consider the spontaneous emission of atomic hydrogen-like emitters into plasmons given by the minimal coupling Hamiltonian,^{34,35}

$$H = H_a + H_{em} + H_{int}, \quad (1)$$

$$H_a = \sum_i \frac{\mathbf{p}_i^2}{2m_e} - \frac{e^2}{4\pi\epsilon_0 r} + H_{e-e} + H_{SO}, \quad (2)$$

$$H_{em} = \sum_{j=x,y,z} \int d\mathbf{r} \int d\omega \hbar \omega \left[f_j^\dagger(\mathbf{r}, \omega) f_j(\mathbf{r}, \omega) + \frac{1}{2} \right], \quad (3)$$

$$H_{int} = \sum_i \frac{e}{2m_e} (\mathbf{p}_i \cdot \mathbf{A}(\mathbf{r}_i) + \mathbf{A}(\mathbf{r}_i) \cdot \mathbf{p}_i) + \frac{e^2}{2m_e} A^2(\mathbf{r}_i) + \frac{e\hbar}{2m_e} \sigma_i \cdot \mathbf{B}(\mathbf{r}_i), \quad (4)$$

with \mathbf{p}_i , \mathbf{r}_i , and σ_i being the impulsion, position, and spin of the i th electron, e being the electronic charge, m_e being the electron mass, \mathbf{A} and \mathbf{B} being the vector potential and magnetic field, H_{SO} being the spin-orbit coupling, and H_{e-e} being the electron-electron interaction. $f_j^\dagger(\mathbf{r}, \omega)$ and $f_j(\mathbf{r}, \omega)$ are the creation and annihilation operators, respectively.

For the interaction Hamiltonian, we neglect the ponderomotive potential (A^2 term) and the \mathbf{B} term as the latter is negligible for non-magnetic structures.³⁶ Note that in the Coulomb gauge, $\nabla \cdot \mathbf{A} = 0$ except at an interface: with the atom-interface distance we consider, and the rapid decay of the atom wavefunctions, the contribution of this term will be negligible. Writing the vector potential with Green's function of the system, and applying the Fermi's golden rule, one finds (for details, see Ref. 5)

$$\Gamma = \frac{2\pi}{\hbar^2} \frac{e^2 \hbar^3}{\pi \epsilon_0 m_e^2 c^2} \iint d\mathbf{r} d\mathbf{r}' \psi_e^*(\mathbf{r}) \psi_e(\mathbf{r}') \nabla \psi_g(\mathbf{r}) \times \text{Im} \vec{G}(\mathbf{r}, \mathbf{r}', \omega_0) \cdot \nabla \psi_g^*(\mathbf{r}'), \quad (5)$$

where ϵ_0 is the vacuum permittivity, c is the speed of light, and ψ_g and ψ_e are the atomic wavefunctions of the ground and excited states of the emitter. $\vec{G}(\mathbf{r}, \mathbf{r}', \omega_0)$ is Green's function of the Maxwell equations and satisfies $\nabla \times (\nabla \times \vec{G}) - \frac{\omega^2}{c^2} \epsilon_r(\mathbf{r}, \omega) \vec{G} = \vec{I} \delta(\mathbf{r} - \mathbf{r}')$, with ϵ_r being the relative permittivity and δ being the delta function.³⁷

Equation (5) computes the transition rates of any emitter (via the atomic wavefunction) within any photonic environment (described by Green's function) in the weak coupling regime. As mentioned, the spatial variation of Green's function is known analytically for uniform media and for simple geometries. However, more complex structures need to be evaluated numerically, with high computational cost.³⁸ Equation (5) is also resource demanding since the integration is performed over six dimensions (\mathbf{r} and \mathbf{r}'). In order to resolve these two issues, we resort to GENOME,²⁹ with the advantage that one modal computation allows the knowledge of the complete spatial Green's function.

In GENOME, the problem is written at a fixed frequency, and the mode-related eigenvalue is the permittivity. This formulation suits well the determination of spontaneous emission rates since the emission frequency is determined by the emitter. The modes $\mathbf{E}_m(\mathbf{r})$ of the scatterer are solved with a commercial finite-element based software (COMSOL Multiphysics),³⁸ and Green's function becomes

$$\vec{G}(\mathbf{r}, \mathbf{r}') = \vec{G}_0(|\mathbf{r} - \mathbf{r}'|) + \frac{1}{k^2} \sum_m \frac{\epsilon_i - \epsilon_b}{(\epsilon_m - \epsilon_i)(\epsilon_m - \epsilon_b)} \mathbf{E}_m(\mathbf{r}) \otimes \mathbf{E}_m^\dagger(\mathbf{r}'), \quad (6)$$

where m is the mode number, k is the vacuum wave vector, ϵ_m is the eigen permittivity, ϵ_i is the permittivity of the scatterer, ϵ_b is the permittivity of the background material, and $\vec{G}_0(|\mathbf{r} - \mathbf{r}'|)$ is Green's function of vacuum, which has an analytical form.³⁷

Inserting Eq. (6) in Eq. (5), we immediately see that the rate is the sum of two contributions $\Gamma = \Gamma_0 + \Gamma_s$, with Γ_0 being the decay rate in vacuum [based on the contribution of $\vec{G}_0(|\mathbf{r} - \mathbf{r}'|)$], and Γ_s depending on the modes and, hence, the nanophotonic structure. Focusing on this Γ_s contribution, we can write

$$\Gamma_s = \frac{2\pi}{k^2} \frac{e^2 \hbar}{\pi \epsilon_0 m_e^2 c^2} \iint d\mathbf{r} d\mathbf{r}' \psi_e^*(\mathbf{r}) \psi_e(\mathbf{r}') \nabla \psi_g(\mathbf{r}) \times \left(\text{Im} \sum_m \gamma_m \mathbf{E}_m(\mathbf{r}) \otimes \mathbf{E}_m^\dagger(\mathbf{r}') \right) \nabla \psi_g^*(\mathbf{r}'), \quad (7)$$

where we defined $\gamma_m = \frac{\epsilon_i - \epsilon_b}{(\epsilon_m - \epsilon_i)(\epsilon_m - \epsilon_b)}$. Note that the adjoint field (\mathbf{E}^\dagger) is the transposed vector and there is no complex conjugate.²⁹

Since we can choose the wavefunctions to be real, the complex conjugate for the wavefunctions disappears and we can integrate separately for \mathbf{r} and \mathbf{r}' . Both integrations give the same value, leading to

$$\Gamma_s = \frac{2\pi}{k^2} \frac{e^2 \hbar}{\pi \epsilon_0 m_e^2 c^2} \sum_m \text{Im} \left[\gamma_m \left(\int \psi_e(\mathbf{r}) \mathbf{E}_m(\mathbf{r}) \nabla \psi_g(\mathbf{r}) d\mathbf{r} \right)^2 \right]. \quad (8)$$

Finally, the transition rates are obtained with a three-dimensional integration over the wavefunctions and the mode profiles, with a sum that can be truncated once the convergence is sufficient (40 modes in our case, see the [supplementary material](#) for more details on the implementation). Note that when the integral is computed, the rate can be known for any material constituting the scatterer, enclosed in the parameter γ_m . In that regard, graphene is the perfect candidate as it can be tuned to match a particular resonance (see Sec. III B).

In this work, the graphene nanoislands are modeled with an effective thickness of $t = 1$ nm. The graphene permittivity (ϵ_i) is deduced from the surface optical conductivity ($\sigma = \tilde{\sigma}_{\text{intra}} + \tilde{\sigma}_{\text{inter}}$) with $\epsilon_i = 1 + i\sigma/\omega\epsilon_0 t$. The optical conductivity is derived within the local random-phase approximation model^{39,40} and is the sum of the following two contributions:

$$\tilde{\sigma}_{\text{intra}} = \frac{2ie^2 k_B T}{\hbar^2 \pi (\omega + i\tau_g^{-1})} \ln \left[2 \cosh \left(\frac{E_F}{2k_B T} \right) \right], \quad (9)$$

$$\tilde{\sigma}_{\text{inter}} = \frac{e^2}{4\hbar} \left[\frac{1}{2} + \frac{1}{\pi} \arctan \left(\frac{\hbar\omega - 2E_F}{2k_B T} \right) \right] - \frac{e^2}{4\hbar} \left[\frac{i}{2\pi} \ln \frac{(\hbar\omega + 2E_F)^2}{(\hbar\omega - 2E_F)^2 + (2k_B T)^2} \right], \quad (10)$$

with $T = 300$ K being the temperature, k_B being the Boltzmann constant, and E_F being the doping level of graphene. The scattering lifetime of electrons in graphene depends on the doping and is given by $\tau_g = \mu E_F / ev_F^2 \approx 10^{-12}$ s for $E_F = 1$ eV, with the impurity-limited DC conductivity $\mu \approx 10\,000$ cm²/(V s) and $v_F = 10^6$ m/s being the graphene Fermi velocity.^{41,42}

The integration of Eq. (8) is successfully compared to direct simulations of dipolar and quadrupolar transitions in the [supplementary material](#), showing great convergence with only 40 modes (1% relative error). In Sec. III, we implement Eq. (8) to compute the rate of a H-like atom close to graphene nanoislands of varying geometry.

III. RESULTS AND DISCUSSION

We apply our method to compute the electric dipolar (E1), quadrupolar (E2), and octupolar (E3) transition rates of a H-like atom close to a graphene sheet with triangle, square, and crescent geometries. We consider the transition series 6p, d, f \rightarrow 4s, which are E1, E2, and E3 transitions, respectively. We suppose that the angular magnetic number remains $m = 0$ during the transition, and we rotate the emitter wavefunctions to match the corresponding classical point-dipole orientation. The free-space wavelengths of the transitions are all $\lambda = 2.63$ μm , and in the whole paper, the emitter is situated 5 nm above the graphene surface.

We then discuss the rate dependence on the graphene doping (Sec. III A) and we demonstrate the advantage of graphene tunability for multipolar transitions (Sec. III B). Finally, we optimize a configuration where the conventional selection rules break down, i.e., when the quadrupolar transition rate dominates the dipolar one (Sec. III C).

A. Transition rates

Figure 1 shows the dipolar (Γ_D), quadrupolar (Γ_Q), and octupolar (Γ_O) transition rates of a H-like emitter in the vicinity of a graphene nanoisland for three geometries: square, triangle, and crescent shape. The rates are normalized by the dipole emission rate in free space, $\Gamma_{D0} = 4.484 \times 10^5 \text{ s}^{-1}$. The latter is obtained by integrating Eq. (5) in free space and is in perfect agreement with the experimental values⁴³ (for more information, see the supplementary material). One can see, for example, that the octupolar rate is strongly enhanced with respect to vacuum: it is up to 300 times stronger than the dipolar rate in free space for the triangle geometry.

One observes that the strongest quadrupolar and octupolar rate enhancements appear along the edges and corners of the geometries. This is a consequence of the strong field gradients appearing along the graphene edge.^{1,44} Second, for all geometries, the

maximum quadrupolar rate is two orders of magnitude smaller than the maximum dipolar rate. This two-order magnitude difference compares fairly with the rate comparison obtained in Ref. 5 for a H-like emitter close to a non-structured two-dimensional material supporting plasmons confined with a factor $\eta_0 \approx 35\text{--}50$ (corresponding to doping between 0.7 and 1 eV). The four-order magnitude difference between the dipolar and octupolar transition rates is also in agreement with the literature.⁵

With the graphene nanoislands, we break the in-plane translational symmetry and the conventional dominance of the dipolar transition rate over the quadrupolar transition rate. From the spatial maps, we observe that the maxima of the quadrupolar rate do not coincide with the maxima of the dipolar rate: by moving the emitter, one can find a position where the quadrupolar rate dominates the dipolar rate, breaking the conventional selection rules (see Sec. III C).

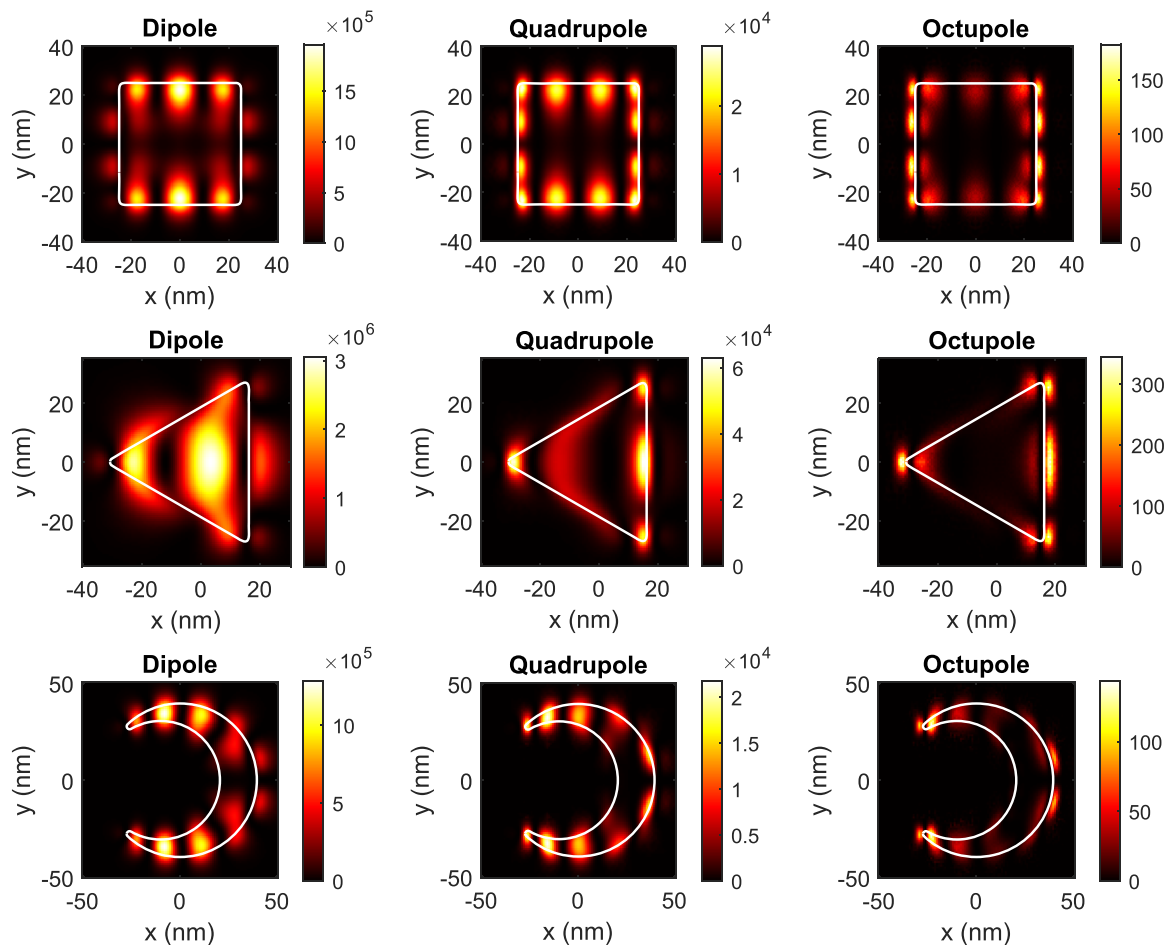


FIG. 1. Dipolar, quadrupolar, and octupolar transition rates of an x-oriented emitter close to graphene nanoislands of various geometries. The dipolar (left), quadrupolar (center), and octupolar (right) transition ($\lambda = 2.63 = \mu\text{m}$) rates as a function of the emitter position, which is 5 nm above the graphene nanoislands: 50 nm side length square (up), 50 nm side length triangle (middle), and 80 nm height crescent (bottom). The geometry boundaries are represented by a solid white line, and the rates are normalized by the dipolar emission rate in free space Γ_{D0} . For all geometries, the background permittivity is vacuum but graphene doping varies: for the triangle, $E_F = 0.98 \text{ eV}$, for the square, $E_F = 0.72 \text{ eV}$, and for the crescent, $E_F = 0.88 \text{ eV}$.

Note that the z -oriented emitter (out-of-plane direction) shows stronger rate enhancement, but the dipolar, quadrupolar, and octupolar transition maxima coincide: they all show the maximum enhancement at the same position (see the [supplementary material](#)). This implies the conservation of selection rules for the z -oriented emitter, as the dipolar rate always dominates.

B. Graphene tunability

In a spontaneous emission process the emission wavelength is fixed via the considered transition. Hence, as the frequency of the source is not a variable, a tuning knob is offered by the environment, e.g., the permittivity of the scatterer. The considered mode expansion is particularly well suited for this context as the permittivity is the eigenvalue of the problem. As a consequence, the permittivity of the scatterer only appears as a multiplicative constant [γ_m factor in Eq. (8)] of the three-dimensional integration over the plasmonic modes (E_m) and the wavefunctions of the emitter. Tuning the permittivity, therefore, allows selecting the mode resonating with the targeted transition.

Figures 2(a)–2(c) show the transition rates' dependence on the permittivity of the material, for a square two-dimensional material with variable permittivity and with a side length of 50 nm. The emitter is y -oriented at the position (14.4; 24.5) nm, 5 nm above the material [green arrow in Figs. 2(d)–2(f)] and the transition wavelength remains $\lambda = 2.63 \mu\text{m}$. The transition rate map is characterized by horizontal lines of enhanced transition rates, appearing at particular relative permittivities of the material [$\text{Re}(\epsilon_r)$]. Each line directly corresponds to a plasmonic mode of the structure, which constitutes the dominant decay route for this transition. For example, the dipolar transition couples with mode A [represented in Fig. 2(d)] and the quadrupolar and octupolar transitions couple with modes B and C [represented in Figs. 2(e) and 2(f)]. Note that modes A and B are different, but their eigenvalues are close (resp. $\epsilon_m = -15.65$ and $\epsilon_m = -15.45$). Their proximity implies that the dipolar rate ($\Gamma_D/\Gamma_{D0} = 1.1 \times 10^5$) dominates the quadrupolar rate ($\Gamma_Q/\Gamma_{D0} = 1.5 \times 10^4$) for the considered position of the emitter, considered emission wavelength, and for a material permittivity close to that particular value [$\text{Re}(\epsilon_r) \approx -15.5$].

Mode C is very interesting since it couples strongly with the quadrupolar transition ($\Gamma_Q/\Gamma_{D0} = 1.2 \times 10^4$) and weakly with

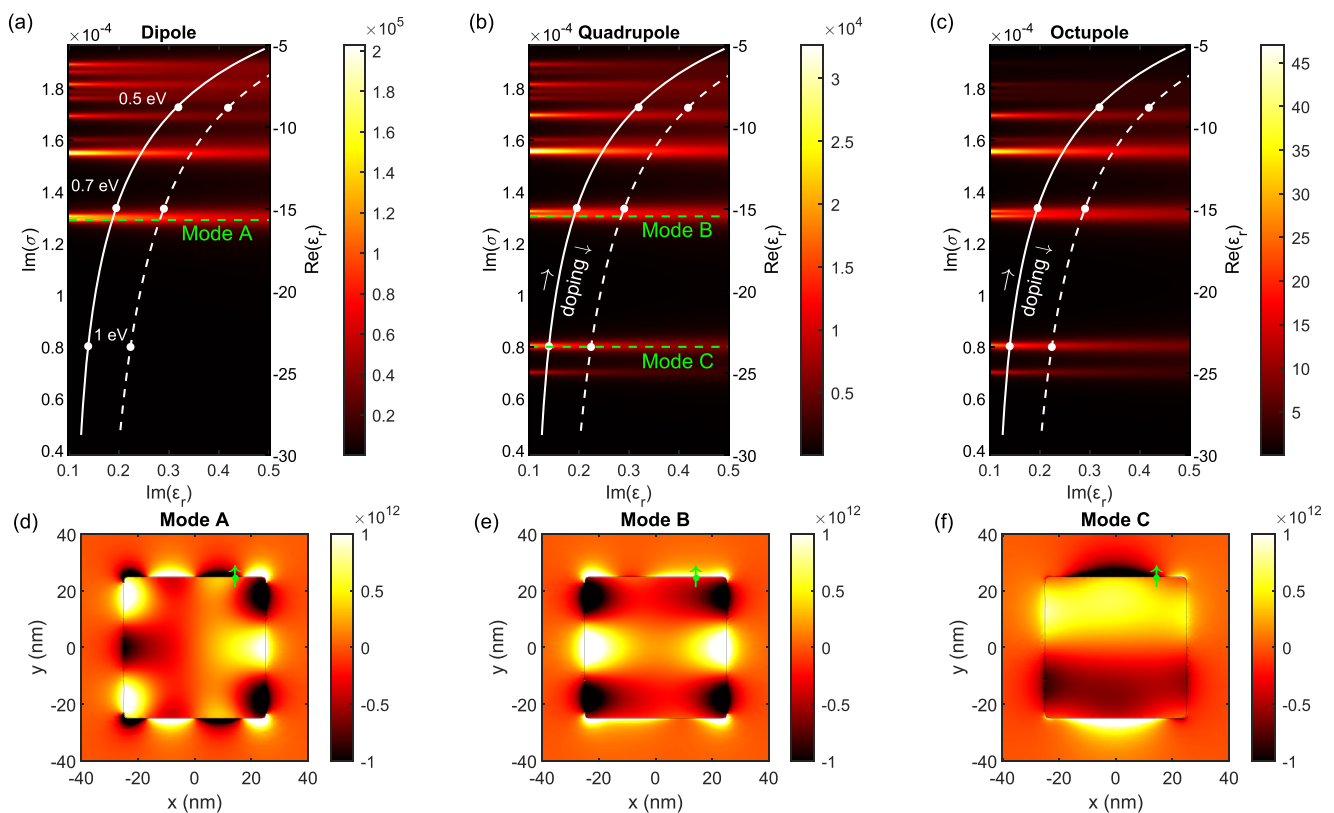


FIG. 2. Choosing the material of the scatterer to enhance particular transition rates. The (a) dipolar, (b) quadrupolar, and (c) octupolar transition ($\lambda = 2.63 \mu\text{m}$) rate enhancement in color scale as a function of the relative permittivity of the scatterer (real and imaginary parts). The imaginary part of the optical conductivity is also represented for more generality. The rates are normalized by the dipolar emission rate in free space. The white line represents the permittivity range covered by graphene upon doping (white dots at 0.5, 0.7, and 1 eV doping) for a DC conductivity of $10\,000 \text{ cm}^2/(\text{V s})$, while the dashed line corresponds to $3000 \text{ cm}^2/(\text{V s})$. The horizontal green dashed lines indicate the modes contributing the most to the considered transition. Their mode profiles (y component of the electric field) are represented in (d) $\epsilon_m = -15.65$, (e) $\epsilon_m = -15.45$, and (f) $\epsilon_m = -23.4$. The green dot and arrow represent the position and orientation of the emitter.

the dipolar transition ($\Gamma_D/\Gamma_{D0} = 0.6 \times 10^3$), as shown in Figs. 2(a) and 2(b). This conclusion corresponds with the field profile in Fig. 2(f) at the position of the dipole (green dot). The emitter is placed at a position where the field has a low value (weak enhancement of dipolar transition), but near the edge, where the field gradient is the strongest (strong enhancement of quadrupolar and octupolar transitions).

In the horizontal direction of Figs. 2(a)–2(c), the imaginary part of the permittivity of the material broadens the resonance peaks, consequently reducing the maximum value of all transition rates.

Therefore, selecting a square two-dimensional material (of this size, and at $\lambda = 2.63 \mu\text{m}$) for a particular permittivity can enhance a particular transition. For example, in order to produce an electric octupolar rate 50 times stronger than the dipolar rate in free space, one can choose a material with real relative permittivity of -23.4 (which corresponds to mode C).

The white lines in Figs. 2(a)–2(c) represent the permittivity range covered by graphene at this wavelength via doping. A fine tuning of the doping thus allows us to select the plasmonic mode that will dominate the transition, and hence the transition order. Note that in the case of lower quality graphene samples, the scattering is enhanced and consequently the DC conductivity can be lowered to $\mu \approx 3000 \text{ cm}^2/(\text{V s})$.⁴² The dashed lines in Figs. 2(a)–2(c) show the permittivity of graphene in this case. The curve is shifted to the right [compared to a DC conductivity is $\mu \approx 10\,000 \text{ cm}^2/(\text{V s})$], which leaves the conclusion unchanged: fine tuning of the doping allows us to select the transition enhancement rates, even if the dipolar, quadrupolar, and octupolar rates are all equivalently reduced by 30%.

In Sec. III C, we show a particular doping of graphene where the quadrupolar rate dominates the dipolar transition rate, consequently breaking the conventional selection rules.

C. Local breakdown of conventional selection rules

At particular positions of the emitter, the quadrupolar transition rate overcomes the dipolar transition rate. This breakdown occurs at ultra-strong plasmon confinement ($\eta_0 > 500$) for planar two-dimensional materials,⁵ which is experimentally achievable with graphene, but at the cost of considerable absorption losses.¹³ The shape of the graphene nanoislands provides another degree of freedom to mold the field profile and break the selection rules.

We focus on the triangular graphene nanoisland of 50 nm side length, for which we computed the normalized dipolar and quadrupolar rates of an emitter 5 nm above its surface (Fig. 1). In Fig. 3(a), we plot the maximum of the ratio Γ_Q/Γ_D (scanned over all positions of the emitter), as a function of the doping. This shows that the quadrupolar transition rate can be up to 100 times stronger than the dipolar transition rate at particular positions, breaking locally the conventional selection rules (the value is converged for 40 modes, as shown in the supplementary material).

In Figs. 3(b) and 3(c), for the x - and y -oriented emitters, respectively, we observe enhancement where the field demonstrates strong gradients, i.e., at the corner of the triangle or along the edge. On the contrary, as observed in Fig. 3(a) for the z -oriented emitter, the dipolar rate always dominates the quadrupolar one (the maximum rate enhancement of each order appears at the same position, as discussed in Sec. III A).

Note that the maximum is not a consequence of an inhibited dipolar transition: the quadrupolar rate is strongly enhanced. For example, for an x -oriented emitter [Fig. 3(b)] at the left corner of the triangle, the dipolar transition remains enhanced ($\Gamma_D/\Gamma_{D0} = 0.51 \times 10^3$), but its rate is weaker than the quadrupolar rate, which is 5.3×10^4 times the dipolar transition in free space.

Other areas further away from graphene seem to demonstrate a strong quadrupolar enhancement [for example, position $(-9; 35) \text{ nm}$

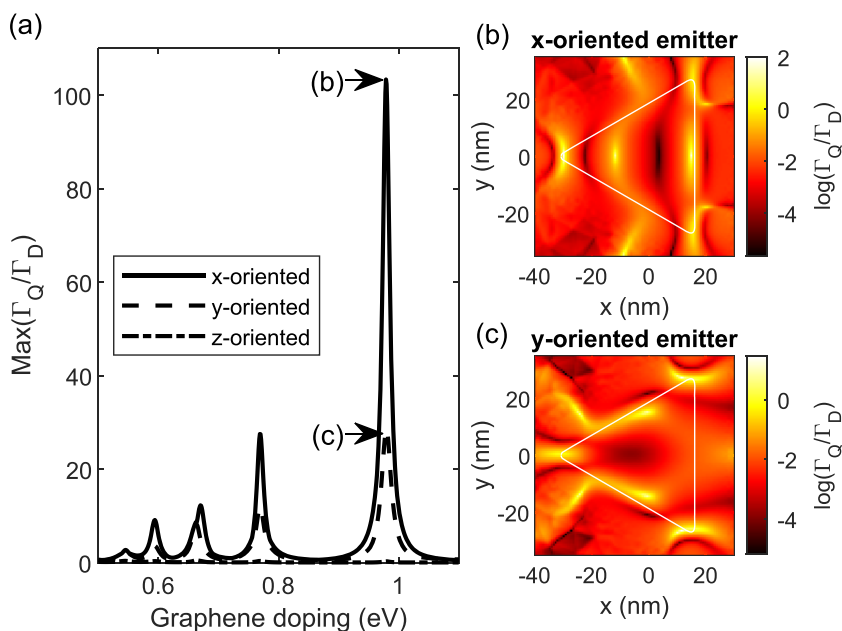


FIG. 3. Local breakdown of the selection rules with the triangle graphene nanoisland. (a) The maximum of the quadrupolar rate (Γ_Q) over the dipolar rate (Γ_D) for a H-like emitter 5 nm above the triangular graphene nanoisland in vacuum, evaluated for varying graphene doping and emitter orientation. The z -oriented emitter does not demonstrate a breakdown of the selection rules (ratio always smaller than 1). A maximum is obtained for a graphene doping of $E_F = 0.98 \text{ eV}$. At this doping, (b) shows the logarithmic value of the ratio for an x -oriented emitter and (c) a y -oriented emitter. The boundaries of the triangular graphene nanoisland are represented by a solid white line and the transition wavelength is $\lambda = 2.63 \mu\text{m}$.

in Fig. 3(b)]. However, these are regions where the dipolar transition is poorly enhanced ($\Gamma_D/\Gamma_{D0} = 16$) as well as the quadrupolar transition ($\Gamma_Q/\Gamma_{D0} = 161$).

IV. CONCLUSIONS AND PERSPECTIVES

We develop a numerical method based on Fermi's golden rule that evaluates the multiple transition orders of a molecule. The molecule is described by its wavefunction, while the photonic environment is implemented through Green's function. The latter is expanded in eigen-permittivity modes leading to a simplified formula [Eq. (8)] that shows the deep mechanism of strong multipolar enhancement. Indeed, the following two main terms play a role in the sum: the global term γ_m and the local term $\int \psi_e(\mathbf{r}) E_m(\mathbf{r}) \nabla \psi_g(\mathbf{r}) d\mathbf{r}$. Together, they show that each mode m contributes to the transition rate. The global term states that the permittivity of the material constituting the nano-island (ϵ_i) should match the mode eigen-permittivity (ϵ_m) to contribute to the transition rate. Hence, graphene is an excellent platform to fit ϵ_i to ϵ_m owing to its optical parameter tunability. The local term shows the primordial importance of the mode field profile locally at the position of the emitter. If the field profile E_m is constant over the spatial extent of the wavefunctions of the emitter (ψ_e and ψ_g), we return to the dipole approximation (or long wavelength approximation), commonly employed in free space, and the higher-order transitions are deemed forbidden. In our case, due to the strong confinement of the field near a graphene nanoisland, the integral is no longer negligible. The order of magnitude of the maximum dipolar, quadrupolar, and octupolar rates compares with the rates obtained for an unstructured graphene sheet⁵ and is in perfect agreement with direct simulations. Finally, we demonstrate a breakdown of the selection rules, with the quadrupolar transition rate, forbidden in free space, becoming 100 times stronger than the dipolar transition rate for an H-like emitter in the vicinity of a triangular graphene nanoisland. These results uncover interesting perspectives for applications in spectroscopy, photochemistry, and quantum technologies.

Here, we apply the method to a single nano-island in free-space, but the method has a large flexibility and can be applied to more realistic structures reachable in experiments. Indeed, GENOME also allows the determination of Green's function for more complex structures. For instance, the method can account for a substrate or a background permittivity different from 1.²⁹ It can also resolve Green's function of non-uniform scatterers.⁴⁵ Recently, the procedure has been developed to find Green's function of an assembly of nano-island (cluster) and finite periodic structures.³⁸ For experimental observations, the coupling of produced photons to the far-field is important. As an example, combining the near-field results (e.g., Fig. 2) with the far-field out-coupling efficiency of the dominant mode allows us to select the graphene doping necessary to reach sufficient far-field emission. Such an analysis was carried out for two-photon emission processes near graphene nanoislands.²⁶ Other structures may be envisaged to enhance the coupling of a plane wave with a quadrupolar transition.⁴⁶

Since the transition of the emitter fixes the operating wavelength, the control of the emitted photons goes through the optimization of the structure and the permittivity of the material. Here, we consider graphene for its tunable properties, already

allowing to target particular transitions (Fig. 2). Strong doping of 1.2 eV has been achieved with electrostatic doping with ionic gel⁴⁷ or with ionic glass mobility⁴⁸ and a moderate doping of 0.5 eV with chemical (N-doped) doping.⁴⁹ It is challenging to reach high Fermi level values, as a specific structure considering the gate and the substrate should be designed. Other materials can also be considered for their strong plasmonic response, such as thin gold films,⁵⁰ or for their strong phononic response, such as hBN or SiC.

In parallel, our method allows for the computation of larger atoms and complex molecules by combining GENOME with time-dependent density functional theory techniques. Hence, controlling the emission rate of quantum dots^{3,6} and Rydberg excitons⁴ in complex electromagnetic environments is within reach. Such emitters are larger than the H-like atoms considered here, so placing those in the gaps of clusters should ensure a strong field gradient over their orbital extent to promote the higher order rate enhancements. Furthermore, since the dipolar and quadrupolar rates compete, destructive interference effects can be observed and lead to suppression of particular transition channels,^{3,21} leading to diverse quantum applications, such as quantum computing, quantum storage, and quantum communication.^{3,21}

SUPPLEMENTARY MATERIAL

See the [supplementary material](#) for details on the method implementation. It contains the integration convergence; a verification of the dipolar transition rate in free-space; a comparison with direct simulations; and additional figures that illustrate the permittivity dependence, the quadrupolar transition rate dominance over the dipolar one for the square graphene nanoisland, and rate calculations for various emitter orientations.

ACKNOWLEDGMENTS

The authors thank Ido Kaminer and Nicholas Rivera for fruitful discussions and Parry Yu Chen and Yonatan Sivan for their support with GENOME. The authors acknowledge support from the FRS-FNRS (Research Project No. T.0166.20 and Grant No. FC 95592) and the Actions de Recherche Concertées, Project No. ARC-21/25 UMONS.

DATA AVAILABILITY

The data that support the findings of this study are available from the corresponding author upon reasonable request.

REFERENCES

- ¹S. Sanders, A. May, A. Alabastri, and A. Manjavacas, "Extraordinary enhancement of quadrupolar transitions using nanostructured graphene," *ACS Photonics* **5**, 3282–3290 (2018).
- ²R. Filter, S. Mühlig, T. Eichelkraut, C. Rockstuhl, and F. Lederer, "Controlling the dynamics of quantum mechanical systems sustaining dipole-forbidden transitions via optical nanoantennas," *Phys. Rev. B* **86**, 035404 (2012).
- ³C. Qian, X. Xie, J. Yang, K. Peng, S. Wu, F. Song, S. Sun, J. Dang, Y. Yu, M. J. Steer, I. G. Thayne, K. Jin, C. Gu, and X. Xu, "Enhanced strong interaction between nanocavities and *p*-shell excitons beyond the dipole approximation," *Phys. Rev. Lett.* **122**, 087401 (2019).

- ⁴A. M. Konzelmann, S. O. Krüger, and H. Giessen, "Interaction of orbital angular momentum light with Rydberg excitons: Modifying dipole selection rules," *Phys. Rev. B* **100**, 115308 (2019).
- ⁵N. Rivera, I. Kaminer, B. Zhen, J. D. Joannopoulos, and M. Soljačić, "Shrinking light to allow forbidden transitions on the atomic scale," *Science* **353**, 263–269 (2016).
- ⁶J. R. Zurita-Sánchez and L. Novotny, "Multipolar interband absorption in a semiconductor quantum dot. I. Electric quadrupole enhancement," *J. Opt. Soc. Am. B* **19**, 1355 (2002).
- ⁷S. Tojo and M. Hasuo, "Oscillator-strength enhancement of electric-dipole-forbidden transitions in evanescent light at total reflection," *Phys. Rev. A* **71**, 012508 (2005).
- ⁸I. D. Rukhlenko, D. Handapangoda, M. Premaratne, A. V. Fedorov, A. V. Baranov, and C. Jagadish, "Spontaneous emission of guided polaritons by quantum dot coupled to metallic nanowire: Beyond the dipole approximation," *Opt. Express* **17**, 17570 (2009).
- ⁹H. Y. Kim and D. S. Kim, "Selection rule engineering of forbidden transitions of a hydrogen atom near a nanogap," *Nanophotonics* **7**, 229–236 (2018).
- ¹⁰V. Yannopoulos and E. Paspalakis, "Giant enhancement of dipole-forbidden transitions via lattices of plasmonic nanoparticles," *J. Mod. Opt.* **62**, 1435–1441 (2015).
- ¹¹T. Neuman, R. Esteban, D. Casanova, F. J. García-Vidal, and J. Aizpurua, "Coupling of molecular emitters and plasmonic cavities beyond the point-dipole approximation," *Nano Lett.* **18**, 2358–2364 (2018).
- ¹²M. Kosik, O. Burlayenko, C. Rockstuhl, I. Fernandez-Corbaton, and K. Slowik, "Interaction of atomic systems with quantum vacuum beyond electric dipole approximation," *Sci. Rep.* **10**, 5879 (2020).
- ¹³Y. Liu, R. F. Willis, K. V. Emtsev, and T. Seyller, "Plasmon dispersion and damping in electrically isolated two-dimensional charge sheets," *Phys. Rev. B* **78**, 201403 (2008).
- ¹⁴A. Woessner, M. B. Lundberg, Y. Gao, A. Principi, P. Alonso-González, M. Carrega, K. Watanabe, T. Taniguchi, G. Vignale, M. Polini, J. Hone, R. Hillenbrand, and F. H. L. Koppens, "Highly confined low-loss plasmons in graphene–boron nitride heterostructures," *Nat. Mater.* **14**, 421–425 (2014).
- ¹⁵N. Rivera, G. Rosolen, J. D. Joannopoulos, I. Kaminer, and M. Soljačić, "Making two-photon processes dominate one-photon processes using mid-IR phonon polaritons," *Proc. Natl. Acad. Sci. U. S. A.* **114**, 13607–13612 (2017).
- ¹⁶S. Tojo, M. Hasuo, and T. Fujimoto, "Absorption enhancement of an electric quadrupole transition of cesium atoms in an evanescent field," *Phys. Rev. Lett.* **92**, 053001 (2004).
- ¹⁷S. Enzonga Yoca and P. Quinet, "Radiative decay rates for electric dipole, magnetic dipole and electric quadrupole transitions in triply ionized thulium (Tm IV)," *Atoms* **5**, 28 (2017).
- ¹⁸W. Li, T. Pohl, J. M. Rost, S. T. Rittenhouse, H. R. Sadeghpour, J. Nipper, B. Butscher, J. B. Balewski, V. Bendkowsky, R. Low, and T. Pfau, "A homonuclear molecule with a permanent electric dipole moment," *Science* **334**, 1110–1114 (2011).
- ¹⁹C.-F. Cheng, Y. R. Sun, H. Pan, J. Wang, A.-W. Liu, A. Campargue, and S.-M. Hu, "Electric-quadrupole transition of H₂ determined to 10⁻⁹ precision," *Phys. Rev. A* **85**, 024501 (2012).
- ²⁰A. Manjavacas, R. Fenollosa, I. Rodriguez, M. C. Jiménez, M. A. Miranda, and F. Meseguer, "Magnetic light and forbidden photochemistry: The case of singlet oxygen," *J. Mater. Chem. C* **5**, 11824–11831 (2017).
- ²¹E. Rusak, J. Straubel, P. Gładysz, M. Göddel, A. Kędziorski, M. Kühn, F. Weigend, C. Rockstuhl, and K. Slowik, "Enhancement of and interference among higher order multipole transitions in molecules near a plasmonic nanoantenna," *Nat. Commun.* **10**, 5775 (2019).
- ²²J. Flick, N. Rivera, and P. Narang, "Strong light-matter coupling in quantum chemistry and quantum photonics," *Nanophotonics* **7**, 1479–1501 (2018).
- ²³A. V. Lavrinenko, J. Lægsgaard, N. Gregersen, F. Schmidt, and T. Søndergaard, *Numerical Methods in Photonics* (CRC Press, 2018).
- ²⁴A. Agrawal, T. Benson, R. M. D. L. Rue, and G. A. Wurtz, *Recent Trends in Computational Photonics*, Springer Series in Optical Sciences Book Vol. 204 (Springer, 2017).
- ²⁵A. Taflove, A. Oskooi, and S. G. Johnson, *Advances in FDTD Computational Electrodynamics: Photonics and Nanotechnology*, Artech House Antennas and Propagation Library (Artech House, 2013).
- ²⁶Y. Muniz, A. Manjavacas, C. Farina, D. A. R. Dalvit, and W. J. M. Kort-Kamp, "Two-photon spontaneous emission in atomically thin plasmonic nanostructures," *Phys. Rev. Lett.* **125**, 033601 (2020).
- ²⁷P. Lalanne, W. Yan, K. Vynck, C. Sauvan, and J.-P. Hugonin, "Light interaction with photonic and plasmonic resonances," *Laser Photonics Rev.* **12**, 1700113 (2018).
- ²⁸D. J. Bergman and D. Stroud, "Theory of resonances in the electromagnetic scattering by macroscopic bodies," *Phys. Rev. B* **22**, 3527–3539 (1980).
- ²⁹P. Y. Chen, D. J. Bergman, and Y. Sivan, "Generalizing normal mode expansion of electromagnetic Green's tensor to open systems," *Phys. Rev. Appl.* **11**, 044018 (2019).
- ³⁰O. D. Miller, A. G. Polimeridis, M. T. Homer Reid, C. W. Hsu, B. G. DeLacy, J. D. Joannopoulos, M. Soljačić, and S. G. Johnson, "Fundamental limits to optical response in absorptive systems," *Opt. Express* **24**, 3329 (2016).
- ³¹D. J. Bergman and M. I. Stockman, "Surface plasmon amplification by stimulated emission of radiation: Quantum generation of coherent surface plasmons in nanosystems," *Phys. Rev. Lett.* **90**, 027402 (2003).
- ³²M. I. Stockman, D. J. Bergman, C. Anceau, S. Brasselet, and J. Zyss, "Enhanced second-harmonic generation by metal surfaces with nanoscale roughness: Nanoscale dephasing, depolarization, and correlations," *Phys. Rev. Lett.* **92**, 057402 (2004).
- ³³K. Li, M. I. Stockman, and D. J. Bergman, "Enhanced second harmonic generation in a self-similar chain of metal nanospheres," *Phys. Rev. B* **72**, 153401 (2005).
- ³⁴S. Scheel and S. Buhmann, "Macroscopic quantum electrodynamics—Concepts and applications," *Acta Phys. Slovaca* **58**, 675 (2008).
- ³⁵D. P. Craig, *Molecular Quantum Electrodynamics: An Introduction to Radiation-Molecule Interactions* (Dover Publications, Mineola, NY, 1998).
- ³⁶J. Sloan, N. Rivera, J. D. Joannopoulos, I. Kaminer, and M. Soljačić, "Controlling spins with surface magnon polaritons," *Phys. Rev. B* **100**, 235453 (2019).
- ³⁷L. Novotny and B. Hecht, *Principles of Nano-Optics* (Cambridge University Press, 2006).
- ³⁸G. Rosolen, B. Maes, P. Y. Chen, and Y. Sivan, "Overcoming the bottleneck for quantum computations of complex nanophotonic structures: Purcell and Förster resonant energy transfer calculations using a rigorous mode-hybridization method," *Phys. Rev. B* **101**, 155401 (2020).
- ³⁹L. A. Falkovsky and A. A. Varlamov, "Space-time dispersion of graphene conductivity," *Eur. Phys. J. B* **56**, 281–284 (2007).
- ⁴⁰L. Falkovsky, "Optical properties of graphene," *J. Phys.: Conf. Ser.* **129**, 012004 (2008).
- ⁴¹J. Christensen, A. Manjavacas, S. Thongrattanasiri, F. H. L. Koppens, and F. J. García de Abajo, "Graphene plasmon waveguiding and hybridization in individual and paired nanoribbons," *ACS Nano* **6**, 431–440 (2012).
- ⁴²K. S. Novoselov, A. K. Geim, S. V. Morozov, D. Jiang, Y. Zhang, S. V. Dubonos, I. V. Grigorieva, and A. A. Firsov, "Electric field effect in atomically thin carbon films," *Science* **306**(5696), 666 (2004).
- ⁴³W. L. Wiese and J. R. Fuhr, "Accurate atomic transition probabilities for hydrogen, helium, and lithium," *J. Phys. Chem. Ref. Data* **38**, 565–720 (2009).
- ⁴⁴V. Karanikolas, P. Tozman, and E. Paspalakis, "Light-matter interaction of a quantum emitter near a half-space graphene nanostructure," *Phys. Rev. B* **100**, 245403 (2019).
- ⁴⁵P. Y. Chen, Y. Sivan, and E. A. Muljarov, "An efficient solver for the generalized normal modes of non-uniform open optical resonators," *J. Comput. Phys.* **422**, 109754 (2020).
- ⁴⁶K. Sakai, T. Yamamoto, and K. Sakai, "Nanofocusing of structured light for quadrupolar light-matter interactions," *Sci. Rep.* **8**, 7746 (2018).
- ⁴⁷A. Paradisi, J. Biscaras, and A. Shukla, "Space charge induced electrostatic doping of two-dimensional materials: Graphene as a case study," *Appl. Phys. Lett.* **107**, 143103 (2015).

⁴⁸D. K. Efetov and P. Kim, “Controlling electron-phonon interactions in graphene at ultrahigh carrier densities,” *Phys. Rev. Lett.* **105**, 256805 (2010).

⁴⁹F. Joucken, L. Henrard, and J. Lagoute, “Electronic properties of chemically doped graphene,” *Phys. Rev. Mater.* **3**, 110301 (2019).

⁵⁰R. A. Maniyara, D. Rodrigo, R. Yu, J. Canet-Ferrer, D. S. Ghosh, R. Yongsunthon, D. E. Baker, A. Rezikyan, F. J. García de Abajo, and V. Pruneri, “Tunable plasmons in ultrathin metal films,” *Nat. Photonics* **13**, 328–333 (2019).